

A COMPUTATIONAL STUDY OF THE INTERFACIAL HEAT TRANSFER IN SPHERICAL AND DEFORMED FLUID PARTICLES

Rafael Franklin Lazaro de Cerqueira, rafaelfc@sinmec.ufsc.br

Emilio Ernesto Paladino, paladino@sinmec.ufsc.br

Róger Mahl, roger@sinmec.ufsc.br

Clovis R. Maliska, mnaliska@sinmec.ufsc.br

Computational Fluid Dynamics Lab

Mechanical Engineering Department - SINMEC, Federal University of Santa Catarina -UFSC, Florianópolis/SC, Brazil

Abstract. *In this paper, the interfacial heat transfer process of spherical and distorted fluid particles is studied through the Volume-Of-Fluid approach, aiming the development of closure correlations for the two-fluid model in heat and mass transfer problems. The Nusselt numbers of spherical particles are compared with the usual correlations presented in literature to validate the numerical model. From the methodology adopted in this work is possible to perform an analysis of the flow and thermal field around the fluid particles and study the effect of different morphologies on the global heat transfer coefficients. It is shown that the interfacial heat flux distribution is affected by the particles shape, inducing changes in the flow and thermal fields around the fluid particle and consequently leading differences in total heat transfer rate.*

Keywords: *Interfacial Heat Transfer, Distorted bubbles, CFD*

1. INTRODUCTION

Gas-liquid two-phase flows are frequently encountered in the oil, chemical and energy transformation industries. Some specific applications in oil and gas industry related to flow assurance problems, such as wax deposition, hydrate formation and corrosion problems by CO₂ and HS₂ among others, require, in addition to the interfacial momentum transfer, the detailed modeling of the heat and mass transfer processes between phases. These flows usually includes multicomponent systems where mass transfer processes are linked to concentration gradients.

Bubbles of different sizes and shapes are encountered in several flow patterns, ranging from spherical ones in finely dispersed bubbly flow to Taylor bubbles in slug flow. Even in slug flow pattern, small dispersed bubbles flow within the liquid slug between two consecutive Taylor bubbles. The simulation of these flows requires precise closure models for interfacial transfer, even in an one-dimensional approaches, utilized in flow wells or multi-dimensional models, employed in the modeling of the flow inside pumps, separators and other elevation components and primary oil treatment. For the case of momentum transfer, several closure relations have been presented in literature (Ishii and Hibiki, 2011; Clift *et al.*, 1978) including correlations for the the cases of distorted bubbles. On the other hand, in modeling interfacial heat and mass transfer processes, in the application of the two fluid models for dispersed flow patterns the usual practice is to employ consolidated correlations based on Re and Pr dimensionless groups, but considering perfectly spherical shaped bubbles (Takemura and Yabe, 1998; Oellrich *et al.*, 1973; LeClair and Hamielec, 1971; Winnikow, 1967), which is not always true in several real applications. Furthermore, the heat and mass transfer between phases in bubbly flow regime is still not fully understood and is a topic of ongoing research (Hayashi *et al.*, 2014; Bothe and Fleckenstein, 2013; Aboulhasanzadeh *et al.*, 2013, 2012; Marschall *et al.*, 2012).

The main difficult in modeling multiphase, multicomponent and non-isothermal flows is the interface tracking and its definition, as well the transfer mechanism and calculation between the two (or more) distinguished domains. Most of the recent numerical works exploring the interfacial heat and mass transfer utilizes interface or front tracking methodologies, such as Volume-Of-Fluid (Bothe and Fleckenstein, 2013), Level-Set (Wang *et al.*, 2008) and other Front-Tracking methods (Aboulhasanzadeh *et al.*, 2012). For the interfacial transfer mechanism, several approaches have been proposed in literature. In the recent paper of Marschall *et al.* (2012), the authors propose a new method for the calculation of the

interfacial mass transfer fluxes, called the Continuous-Species-Transfer(CST) which is based on an analogy of the the well-known Continuous-Surface-Force(CSF) Method from Brackbill *et al.* (1992). Another alternative to calculate the mass and heat transfer is to utilize the overall energy or mass balance concept, as showed in (Hase and Weigand, 2004) and (Wang *et al.*, 2008).

The main objective of the present work is to determine, through a detailed modeling of the flow around bubbles with different interface shapes, the interfacial heat and mass transfer coefficients in non-isothermal multiphase flows and how the interface shape affects the process and, ultimately, the global heat and mass transfer coefficients, which are needed for the two-fluid model closure.

2. METHODOLOGY

2.1 CFD model

To accomplish the objective previously defined, the detailed flow structure around individual bubbles was studied through the Coupled Level Set and Volume-of-Fluid (CLSVOF) method (Sussman and Puckett, 2000). In this approach the advantages of the Level Set method (well defined interface and easiness of computing its curvature) and the Volume-Of-Fluid method (naturally conservative) are combined.

For the momentum equation, the chosen surface stress model was the Continuous Surface Force (CSF) (Brackbill *et al.*, 1992). The phases are modeled as incompressible and viscous in a laminar flow. The simulations presented in this work were developed in ANSYS FLUENT CFD 15.0.

From the generalized graphical correlation shown in (Clift *et al.* (1978), p. 27) the bubble shape can be predicted by the use of some characteristic dimensionless numbers, these are the Eötvös ($Eo = g(\rho_c - \rho_b)d_b^2/\sigma$), Reynolds ($Re = \rho_c U_{tb} d_b / \mu_c$) and Morton ($Mo = g\mu_c^4(\rho_c - \rho_b) / \rho_c^2 \sigma^3$), where ρ is the density, μ is the viscosity, σ is the surface tension, U_{tb} is the bubble terminal velocity, d_b is the bubble diameter, whose calculation will be shown later. The subscripts b and c represent, the bubble and the continuous phase, respectively.

Another important dimensionless number in the heat transfer analysis is the Prandtl number ($Pr = C_{p_c} \mu_c / k_c$) that gives the relation of momentum and thermal diffusivity.

Along with fore mentioned dimensionless numbers, four other characteristic dimensionless numbers are the density ratio ($\gamma = \rho_b / \rho_c$), the viscosity ratio ($\kappa = \mu_b / \mu_c$), the thermal conductivity ratio ($\beta = k_b / k_c$) and the specific heat capacity ratio ($\lambda = C_{p_b} / C_{p_c}$)

In the analysis of the heat transfer between the phases, the results presented in this work will be expressed by the Nusselt number ($Nu = h d_b / k_c$), where h is the heat transfer coefficient.

In a heat transfer analysis, the common practice to obtain the heat transfer coefficient h value is to employ a heat balance at the interface in the following manner,

$$h = \frac{-k_c}{S \Delta T} \left. \frac{\partial T}{\partial \hat{n}} \right|_{\text{interface}} \quad (1)$$

where \hat{n} is normal vector pointing outward the interface, ΔT is the temperature difference and S is the interfacial surface area.

However, one of the shortcomings of the interface tracking through implicit methods, such as VOF, Level-Set or CLSVOF, is that the interface position is not exactly defined. Although the mesh refinement lead to a more accurate capture of the interface position, from the continuous point of view of the VOF approach, the high gradients of both temperatures and, mainly, fluid transport properties, which, when evaluated for the mixture, are function of the volume fraction, happens precisely at the interfacial region. Thus the explicit calculation of the interfacial heat fluxes is not accurate, as can be seen in Fig. 1 where the dimensionless local Nusselt (Eq. (9)), tangential velocity (Eq. (10)) along the interfaces (calculated with $\phi = 0.00$, $\phi = 0.01$ and $\phi = 0.02$) are given. As seen, the interface position and the velocity profiles show almost none discrepancies, while the local Nusselt for the three ϕ values do not coincide at the particles

front hemisphere, where the heat fluxes are stronger. Although the values are not the same, they show the same tendency and are of fundamental importance to support the physical analysis and conclusions about the global results obtained.

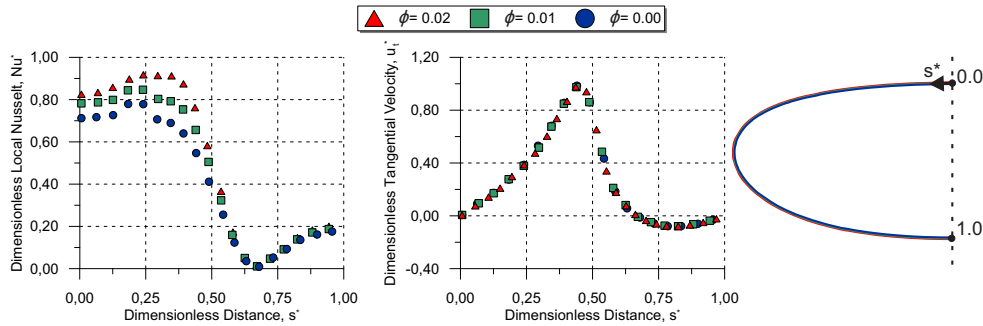


Figure 1. Dimensionless local Nusselt number Nu^* and dimensionless tangential velocity u_t^* for the interfaces obtained for different Level-set function ϕ values.

The calculation of the interfacial heat fluxes are also a difficulty in explicit interface tracking methods, as Lagrangian approaches based on immersed boundary methods (Aboulhasanzadeh *et al.*, 2012; Hayashi *et al.*, 2014), as the transport equations are resolved in a fixed the background mesh where the fluxes at the interface cannot be explicitly calculated, even when the position of the interface is explicitly determined, as any of these methods cannot handle sharp variation of the transport properties. The only approaches which allows the explicit calculation of interfacial fluxes are those based on the interface fitted grid.

In addition, when calculating the heat transfer coefficient h (Eq. (1)) a reference temperature is required at the interface, T_s . Once the temperature variation across the interfacial region is sharp in the CLSVOF method, the interfacial temperature T_s cannot be easily defined. This problem was tackled by calculating the Nu number from a global balance, maintaining the particle temperature by the inclusion of a source term in the energy conservation equation, via FLUENT's User Defined Functions(UDF), which was equal to the total heat transferred in the previous timestep Δt , from the bubble to the continuous phase. Equation (2) is the source term added to the energy conservation equation

$$S_h = \frac{\alpha_b \rho_b C_{Pb} (T_b - T^{t-\Delta t})}{\Delta t} \quad (2)$$

where T_b is the bubble temperature defined in the beginning of each simulation run and $T^{t-\Delta t}$ is the temperature in the previous timestep. The term α_b in Eq. (2) ensures that the source term only exists in the bubble domain, seeing that α_b has zero value outside bubble domain and $0 < \alpha_b \leq 1$ inside.

With the aid of this source term, T_b remained constant during the whole simulation time due to the fact that a small time step Δt was chosen. As a result, the reference temperature difference ($\Delta T = T_b - T_c$) was simply made equal to the temperature of the bubble T_b minus the temperature of the liquid far from the interface T_c (which is equal to the initial liquid temperature). Employing an energy balance in a control volume $V.C.$ large enough to enclose the bubble interface, it was possible to calculate the total heat \dot{Q} transferred from the dispersed to the continuous phase through the integration of S_h resulting in $\dot{Q} = \int_{V.C} S_h dV$. In this fashion, the Nusselt number, is defined by

$$Nu = \frac{\dot{Q} d_b}{S (T_b - T_c) k_c} \quad (3)$$

The analysis of the local Nusselt number along the interface is important in order to understand some phenomena related to local flow pattern as, for instance, the separation point of the boundary layer, behind the fluid particle. The local Nusselt number was calculated through the explicit calculation of the interfacial fluxes assuming an interface position, which is defined as the iso-surface where the level-set function had zero value ($\phi = 0.00$). The convective heat

transfer coefficient h was calculated with Eq. (1), and then, the resulting Nusselt number was non-dimensionalized by the difference between the maximum and minimum values of the Nu number (Eq. (9)). Although the resulting Nu numbers calculated in this way can be only considered as qualitative parameters, as the same methodology was used in all cases, a qualitative comparison of local phenomena, among the different cases can be performed.

To simulate the process of a rising bubble in a infinite media, the computational domain and the boundary conditions were defined according to the scheme shown in Fig. 2.

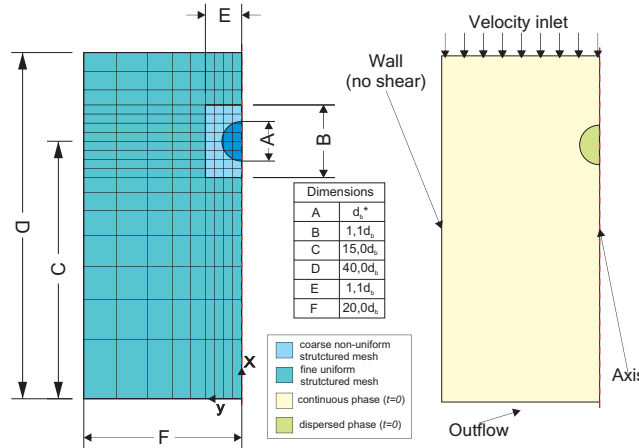


Figure 2. Computational domain scheme, boundary and initial conditions.

In this work, the governing equations are solved with the reference coordinate system fixed on the bubble. Employing this reference coordinate system, it was possible to reduce the computational domain, once it was only needed to enclose a relative small domain around the bubble, when comparing the computational domain required for a inertial coordinate system. This allowed for a better mesh refinement, specially near the bubble, where the transfer of heat and momentum occurs, enhancing the quality of the results and allowing the bubble to rise for large periods of time with no physical limitation.

In order to include the effects of the bubble acceleration, a source term was added to the momentum conservation equation via FLUENT's User Defined Functions(UDF). First, an average bubble rise velocity U_b^t was calculated, in a instant of time t as

$$U_b^t = \frac{\int_{\phi \leq 0} u d\Omega}{\int_{\phi \leq 0} d\Omega} \quad (4)$$

where Ω is the computational domain and u is the axial component of velocity \vec{u} . It is important to leave clear, that the volumes with $\phi \leq 0$ where approximately the ones enclosing the dispersed phase (bubble) and the calculations were performed after each time step was converged. This U_b^t was then introduced to the U_{inlet} as $U_{inlet} = -U_b^t$ in the top boundary condition (see Fig.2) at the new instant of time $t + \Delta t$. A new average bubble rise velocity $U_b^{t+\Delta t}$ was obtained at this time instant. The bubble acceleration in each time step was evaluated as,

$$a_{bubble} = \frac{U_b^{t+\Delta t} - U_b^t}{\Delta t} \quad (5)$$

In this way, the source term introduced in the momentum conservation equation $S_m = -\rho a_{bubble}$ and was applied to each volume of the computational domain to remain the bubble stationary.

For the cases of deformed bubble shapes, it was necessary to define an equivalent bubble diameter to obtain some of the dimensionless parameters presented in the equations above. This bubble diameter d_b was defined as the equivalent

diameter from a spherical bubble, such that

$$d_b = \sqrt[3]{\frac{6V_s}{\pi}} \quad (6)$$

derived from the volume from a sphere ($\pi d^3/6$) and a calculated bubble volume V_s .

To simulate the rising bubble, the bubble initial shape was defined as a sphere with diameter d_b placed $15d_b$ away from the bottom. In the interest to reduce the computational effort, the mesh was subdivided in two different regions, a smaller fine region with an uniform structured mesh followed by a larger coarse non-uniform structured mesh. The transition between the regions was made smooth with the help of a spline function.

2.2 Numerical Simulations

In order to study the effect of the bubble shape on the heat transfer process, it was necessary to develop studies for situations located in the three distinct regions of the bubble shape regimes: i) spherical; ii) ellipsoidal and iii) ellipsoidal-cap, as presented (Clift *et al.* (1978), p. 27).

The simulations were performed for a pair of Eötvös Eo and Morton Mo numbers with three different Pr values ($Pr = 5.0$, $Pr = 7.5$ and $Pr = 10.0$). The property ratios were set constant for all cases ($\kappa = \gamma = \lambda = \beta = 0.1$).

3. NUMERICAL PROCEDURE

3.1 Mesh convergence test

A mesh refinement study was made to ensure that simulations were performed free of discretization error and the computational mesh was capable to capture the boundary layer effects, once the interfacial heat and momentum transfer occurs in this region.

Based on the fact that higher the Re , thinner is the momentum boundary layer and the Pr number gives the relation of the momentum and thermal boundary layer in a inverse proportion, i.e. higher the Pr , smaller is the thermal boundary layer, the mesh convergence study was made for the higher Mo in each Eo – the higher Re in each Eo – with $Pr = 10.0$.

The number of volumes accounted in the mesh refinement study are those of the fine region (see Fig. 2), $N_{vol} = (1.1d_b)(1.1d_b)/\Delta l^2$, where $\Delta l = \Delta x = \Delta y$ is the finite volume size in the fine region. Below in Fig. 3 is the Nu values for the different mesh sizes.

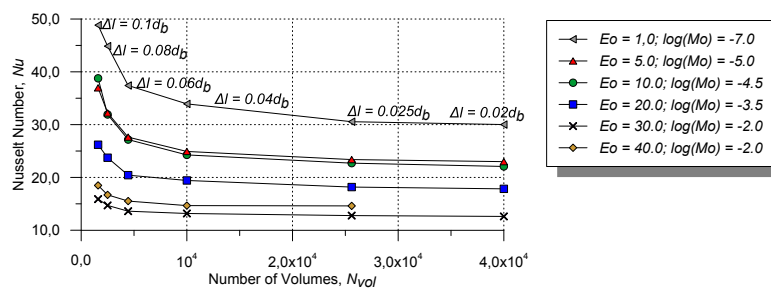


Figure 3. Mesh convergence study for the higher Re in each Eo with $Pr = 10.0$.

Figure 3 shows that the mesh resolution with $\Delta l = 0.04d_b$ presents little deviation from the finer resolution, except for $Eo = 1.0$. This exception can be explained by the high Re number of this point, greater than the other simulations. Therefore, for $Eo = 1.0$ the simulations were performed with $\Delta l = 0.02d_b$ while for the others $\Delta l = 0.04d_b$.

4. RESULTS AND DISCUSSIONS

4.1 Comparison with the literature

From the spherical and almost spherical (for high Re values the morphology slightly deviates from a sphere) cases presented ($Eo = 1.0$), the numerical results presented here were compared with correlations found in literature (Takemura and Yabe, 1998; Oellrich *et al.*, 1973; LeClair and Hamielec, 1971; Winnikow, 1967). This comparison is shown in Fig. 4 for $Pr = 10.0$ through the Nusselt number Nu and the Nu_{diff} (see Eq. (7)) plotted against the obtained Re number. The results for $Pr = 5.0$ and $Pr = 7.5$ presented the same behavior, an increase in Re leading to an increase in Nu .

$$Nu_{diff} = \frac{Nu - Nu_{corr}}{Nu}, \quad (7)$$

where Nu_{corr} is the value given by the correlations found in the literature.

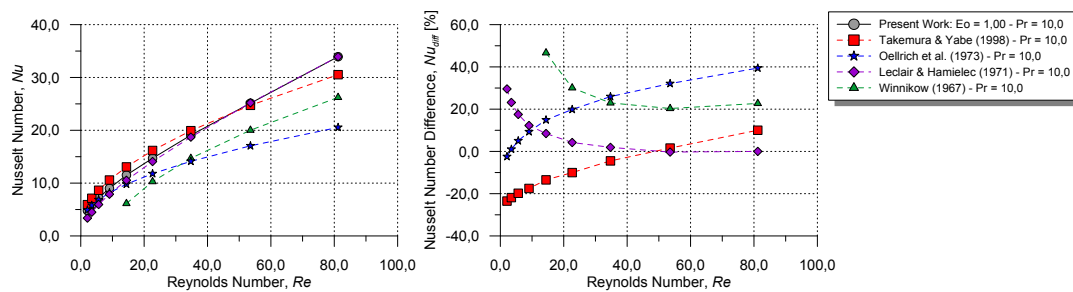


Figure 4. Nusselt Nu and Nu_{diff} (see Eq. (7)) values against Reynolds Re numbers obtained in the present work from correlations found in literature (Takemura and Yabe, 1998; Oellrich *et al.*, 1973; LeClair and Hamielec, 1971; Winnikow, 1967) for $Pr = 10.0$.

From Fig. 4 it is possible to see that the methodology utilized in the present work captures well the interfacial transfer and agree well with the correlations presented. As expected, the increase in the Reynolds Re number provokes an increase in the Nusselt Nu number and $Nu \rightarrow 2.0$ for $Re \rightarrow 0$, the value for pure diffusive heat transfer.

4.2 Local Heat Transfer

Figure (5) shows the bubbles shape, temperature and the external and internal flow streamlines, after reaching the steady-state regime, for four different configurations. The morphologies can be classified as the following: i) spherical shape ($Eo = 1.0, \log(Mo) = -5.0$); ii) ellipsoidal shape ($Eo = 5.0, \log(Mo) = -5.0$ and $Eo = 10.0, \log(Mo) = -4.5$); and iii) ellipsoidal-cap shape ($Eo = 40.0, \log(Mo) = -2.0$).

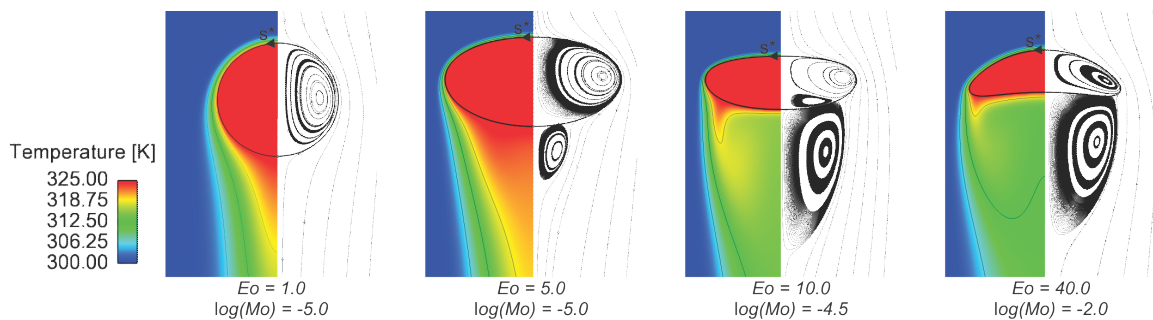


Figure 5. Bubble shape, temperature and the streamlines around and inside it, after reaching the steady-state regime for $Pr = 10.0$ (not in scale).

Figure 5 gives a visual insight of how the deformation (deviation from the spherical shape) affects the temperature

field and flow around and inside the fluid particle domain. As the deformation increases (higher Eo) a recirculation zone starts to appear in the rear, affecting the temperature field in this region.

In order to show how the deviation from a spherical shape and the velocity field near the interface affects the heat transfer, Fig. 6 gives the normalized Nusselt number Nu^* and normalized tangential interface velocity u_t^* around the bubble with the aid of the dimensionless distance s^* , these denoted by:

$$s^* = \frac{s}{s_{\max}}; \quad (8)$$

$$Nu^* = \frac{Nu_{loc} - Nu_{\min}}{Nu_{\max} - Nu_{\min}}; \quad (9)$$

$$u_t^* = \frac{|u_{tloc}|}{u_{t\max}}; \quad (10)$$

where \vec{t} is the tangential interface vector of bubble interface and the subscripts loc, min and max refers respectively to the local, minimum and maximum values.

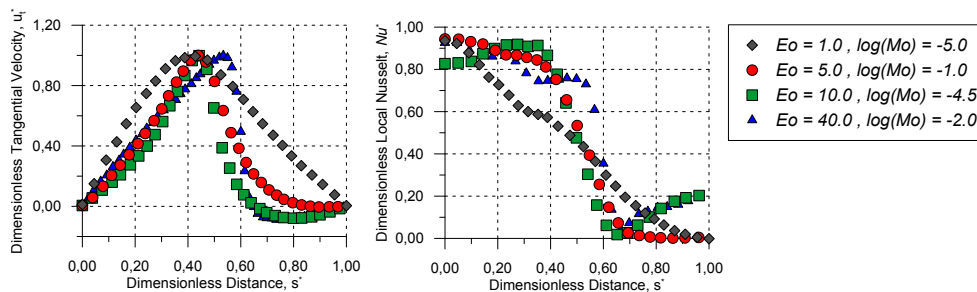


Figure 6. Normalized tangential interface velocity u_t^* and Nusselt number Nu^* around the bubble. These profiles were extracted for the situations given in Fig. 5.

From Fig. 6 the wake region is clearly visible in the s^* vs. u_t^* plot, comprehending the region where u_t^* changes its sign. The effects of this recirculation and the fluid particle morphology in the interfacial heat transfer is also seen in the s^* vs. Nu^* plot. For $Eo = 1.0$, a case that does not have recirculating fluid, the local interfacial heat transfer decays from a maximum value in the bubble front ($s^* = 0.00$) to a minimum in the rear end ($s^* = 1.00$). Increasing the Eo , $Eo = 5.0$, the profile begins to change, with the recirculation zone lowering the heat transfer in the rear. In the front position, the heat transfer is augmented by the flattening of his region. In the two last situations, $Eo = 10.0$ and $Eo = 40.0$, the recirculation behind the fluid is more intense, allowing the bubble to exchange more heat when compared to the last situation ($Eo = 5.0$). For $Eo = 10.0$, the maximum interfacial heat transfer is no longer placed in the front stagnation point, but next to the maximum u_t^* position due of the flattening of the north hemisphere. This maximum point returns to front stagnation point for $Eo = 40.0$ due to the "streamlined" shape of the ellipsoidal-cap.

5. CONCLUSIONS

In this work the interfacial heat transfer of spherical and distorted bubbles was studied with the Coupled Level Set and Volume-Of-Fluid (CLSVOF) model available in ANSYS CFD FLUENT 15.0. The governing equations were solved for a moving reference frame, including the effect of the bubble acceleration trough a source term in the momentum conservation equation, implemented via FLUENTs User Define Functions (UDF).

It is shown that is difficult to evaluate temperatures and fluxes in the interface, due to shortcoming of the interface tracking through implicit methods, although the values obtained in this fashion present qualitative results. In order to compensate for this fact, the temperature in the dispersed phase (bubble) is maintained constant through an energy source term added via FLUENTs User Define Functions (UDF). With the aid this source term is possible to calculate the interfa-

cial heat transfer and to develop studies from different bubble regimes.

The methodology utilized in the present work capture well the interfacial transfer, once the mesh refinement study shows that the boundary and momentum boundary layer are captured and the dimensionless values obtained (Nu and Re) agree well with correlations encountered in the literature (Takemura and Yabe, 1998; Oellrich *et al.*, 1973; LeClair and Hamielec, 1971; Winnikow, 1967) for spherical bubbles.

Through a detailed modeling and analysis of the flow around bubbles with different shapes it was possible to perceive changes in the thermal and flow behavior as the deviation from a spherical shape increases.

6. ACKNOWLEDGMENTS

This work was realized with the financial support of the Brazilian National Petroleum Agency - ANP, through the Human Resources Program of ANP for Petroleum and Natural Gas.

7. REFERENCES

- Aboulhasanzadeh, B., Hosoda, S., Tomiyama, A. and Tryggvason, G., 2013. "A validation of an embedded analytical description approach for the computations of high schmidt number mass transfer from bubbles in liquids". *Chemical Engineering Science*, Vol. 101, pp. 165–174.
- Aboulhasanzadeh, B., Thomas, S., Taeibi-Rahni, M. and Tryggvason, G., 2012. "Multiscale computations of mass transfer from buoyant bubbles". *Chemical Engineering Science*, Vol. 75, pp. 456–467.
- Bothe, D. and Fleckenstein, S., 2013. "A volume-of-fluid-based method for mass transfer processes at fluid particles". *Chemical Engineering Science*, Vol. 101, No. 0, pp. 283 – 302.
- Brackbill, J., Kothe, D.B. and Zemach, C., 1992. "A continuum method for modeling surface tension". *Journal of computational physics*, Vol. 100, No. 2, pp. 335–354.
- Clift, R., Grace, J. and Weber, M., 1978. "Bubbles". *Drops and Particles (Academic, New York, 1978)*, p. 1870.
- Hase, M. and Weigand, B., 2004. "Transient heat transfer of deforming droplets at high reynolds numbers". *International Journal of Numerical Methods for Heat & Fluid Flow*, Vol. 14, No. 1, pp. 85–97.
- Hayashi, K., Hosoda, S., Tryggvason, G. and Tomiyama, A., 2014. "Effects of shape oscillation on mass transfer from a taylor bubble". *International Journal of Multiphase Flow*, Vol. 58, pp. 236–245.
- Ishii, M. and Hibiki, T., 2011. *Thermo-fluid dynamics of two-phase flow*. Springer.
- LeClair, B. and Hamielec, A., 1971. "Viscous flow through particle assemblages at intermediate reynolds numbers – a cell model for transport in bubble swarms". *The Canadian Journal of Chemical Engineering*, Vol. 49, No. 6, pp. 713–720.
- Marschall, H., Hinterberger, K., Schueler, C., Habla, F. and Hinrichsen, O., 2012. "Numerical simulation of species transfer across fluid interfaces in free-surface flows using openfoam". *Chemical Engineering Science*, Vol. 78, pp. 111–127.
- Oellrich, L., Schmidt-Traub, H. and Brauer, H., 1973. "Theoretische berechnung des stofftransports in der umgebung einer einzelblase". *Chemical Engineering Science*, Vol. 28, No. 3, pp. 711–721.
- Sussman, M. and Puckett, E.G., 2000. "A coupled level set and volume-of-fluid method for computing 3d and axisymmetric incompressible two-phase flows". *Journal of Computational Physics*, Vol. 162, No. 2, pp. 301–337.
- Takemura, F. and Yabe, A., 1998. "Gas dissolution process of spherical rising gas bubbles". *Chemical engineering science*, Vol. 53, No. 15, pp. 2691–2699.
- Wang, J., Lu, P., Wang, Z., Yang, C. and Mao, Z.S., 2008. "Numerical simulation of unsteady mass transfer by the level set method". *Chemical Engineering Science*, Vol. 63, No. 12, pp. 3141–3151.
- Winnikow, S., 1967. "Letter to the editors". *Chemical Engineering Science*, Vol. 22, No. 3, pp. 477 –.

8. RESPONSIBILITY NOTICE

The authors are the only responsible for the printed material included in this paper.